AGU PUBLICATIONS

JGR

Journal of Geophysical Research: Oceans

RESEARCH ARTICLE

10.1002/2015JC011133

Key Points:
- The East Australia Current separates at 34°S
- Controls on fate of water are investigated
- Depth of water is main control, with deep water flowing south

Correspondence to:
S.L. Ypma,
s.l.ypma@tudelft.nl

Citation:
Ypma, S. L., E. van Sebille, A. E. Kiss, and P. Spence (2016), The separation of the East Australian Current: A Lagrangian approach to potential vorticity and upstream control, *J. Geophys. Res. Oceans*, *121*, 758–774, doi:10.1002/2015JC011133.

Received 11 JUL 2015
Accepted 18 DEC 2015
Accepted article online 22 DEC 2015
Published online 22 JAN 2016

The separation of the East Australian Current: A Lagrangian approach to potential vorticity and upstream control

S. L. Ypma[1,2,3,4], E. van Sebille[1,3,5], A. E. Kiss[4,6], and P. Spence[3,4]

[1]Institute for Marine and Atmospheric Research Utrecht, Utrecht University, Utrecht, Netherlands, [2]Now at Environmental Fluid Mechanics Section, Faculty of Civil Engineering and Geosciences, Delft University of Technology, Delft, Netherlands, [3]Climate Change Research Centre, University of New South Wales, Sydney, New South Wales, Australia, [4]ARC Centre of Excellence for Climate System Science, Sydney, New South Wales, Australia, [5]Department of Physics, Grantham Institute, Imperial College, London, UK, [6]School of Physical, Environmental and Mathematical Sciences, University of New South Wales Canberra at the Australian Defence Force Academy, Canberra, Australian Capital Territory, Australia

Abstract The East Australian Current (EAC) is the western boundary current flowing along the east coast of Australia separating from the coast at approximately 34°S. After the separation two main pathways can be distinguished, the eastward flowing Tasman Front and the extension of the EAC flowing southward. The area south of the separation latitude is eddy-rich and the separation latitude of the EAC is variable. Little is known of the properties of the water masses that separate at the bifurcation of the EAC. This paper presents new insights from the Lagrangian perspective, where the water masses that veer east and those that continue south are tracked in an eddy-permitting numerical model. The transport along the two pathways is computed, and a 1:3 ratio between transport in the EAC extension and transport in the Tasman Front is found. The results show that the "fate" of the particles is to first order already determined by the particle distribution within the EAC current upstream of the separation latitude, where 85% of the particles following the EAC extension originate from below 460 m and 90% of the particles following the Tasman Front originate from the top 460 m depth at 28°S. The separation and pathways are controlled by the structure of the isopycnals in this region. Analysis of anomalies in potential vorticity show that in the region where the two water masses overlap, the fate of the water depends on the presence of anticyclonic eddies that push isopycnals down and therefore enable particles to travel further south.

1. Introduction

The separation of the East Australian Current (EAC), the western boundary current flowing southward along the east coast of Australia, plays a dominant role in the flow pattern within the Tasman Sea. While transporting heat and biota from the Coral Sea to the Tasman Sea, the EAC separates into an eastward current at approximately 34°S known as the Tasman Front and a southward branch forming the EAC extension [e.g., *Godfrey et al*., 1980a; *Ridgway and Dunn*, 2003]. Volume transports of both pathways have been previously estimated at ∼9.7 Sv for the extension of the EAC [*Oliver and Holbrook*, 2014] and between −4 and 18 Sv for the Tasman Front [*Sutton and Bowen*, 2014], although the highly variable nature of the pathways' strength and location makes accurate estimates difficult. The EAC current system is highly variable and dynamic, with a ratio of eddy kinetic energy to mean kinetic energy of 500:1 compared to 10:1 in the global average [e.g., *Mata et al*., 2006; *Scharffenberg and Stammer*, 2010; *Everett et al*., 2012].

The Tasman Front is a surface-intensified flow that is confined to the upper 800 m [*Sutton and Bowen*, 2014]. The front is shallower than the EAC, which itself extends to a depth below 2000 m. *Sutton and Bowen* [2014], using a yearlong deployment of current meters in a moored array deployed south of Norfolk Island, hypothesize that part of the deeper water of the EAC that does not flow along the Tasman Front, forms leakage past the southern tip of Tasmania toward the Indian Ocean. Model studies show that this Tasman Leakage, fed by the extension of the EAC, is located in the upper 1000 m of the ocean and its core is centered around 100 m depth [*Van Sebille et al*., 2012]. Whether this water indeed originates from the deeper part of the EAC has not yet been investigated.

From previous studies, three main theories concerning the separation of the EAC can be distinguished. First, observations of the EAC region show that the separation of the EAC often takes place near Sugarloaf Point at 32.4°S, where the coastline has a strong curvature [*Godfrey et al*., 1980a]. This suggests that the separation is topographically controlled. Indeed, *Marchesiello and Middleton* [2000], using a vorticity balance model, find that a bend in the continental slope is the determinant factor that causes the EAC to separate in combination with the forcing from baroclinic Rossby waves. However, other studies argue that Rossby waves are not the main players in controlling the formation of the EAC eddies and that the variability in the EAC region is generated locally around the separation latitude [*Bowen et al*., 2005; *Mata et al*., 2006].

In contrast, *Tilburg et al*. [2001] argue that bottom topography and coastline details have little effect on the separation latitude. Using numerical simulations whose complexity is systematically increased, they find that the inclusion of wind forcing results in the correct separation latitude, where gradients in the zonally integrated wind stress curl field determine the location. Analysis of sediment cores from the Coral Sea and the Tasman Sea show that during the last glacial period the EAC separation took place between 23°S and 26°S [*Bostock et al*., 2006], approximately 10° further north relative to present-day observations. *Bostock et al*. [2006] mention the possibility that the shift is caused by a change in the wind stress curl field in the last glacial period. Furthermore, *Oliver and Holbrook* [2014], using climate change simulations of the Tasman Sea circulation, show that the separation latitude may shift 100 km southward from 1990 to 2060. *Oliver and Holbrook* [2014] argue that the linear Sverdrup theory cannot explain the southward shift and that the mean location of the separation is governed by baroclinic, eddy-rich dynamics. Additionally, a shift in the separation latitude suggests that the dynamics of the separation latitude is not only purely controlled by topography.

Lastly, the separation of a western boundary current can also occur for reasons of vorticity dynamics, even in the absence of changes in the wind stress curl, bathymetry, or a curvature of the coastline [*Kiss*, 2002]. Under no-slip boundary conditions the potential vorticity of the cyclonic near-shore part of the western boundary current becomes larger than the potential vorticity of the interior. *Kiss* [2002] shows that the excess potential vorticity can only be dissipated by an outflow separating from the coast. This theory has been extended to idealized turbulent, stratified gyres [*Kiss*, 2010] and used to explain Kuroshio separation in oceanic general circulation models [*Nakano et al*., 2008].

The different theories of why the EAC separates where it does show the complexity of the western boundary current systems and the different mechanisms that affect their separation point. A complete description of the variability of the EAC separation will likely need to take all forcing mechanisms mentioned above into account. Modeling a realistic western boundary current separation is very sensitive to choices made for subgrid-scale parameterizations and a proper representation of water mass properties, bathymetry, and air-sea fluxes. Despite the long history of research on modeling western boundary currents, there is not yet a single recipe that guarantees a correct separation of all western boundary currents in a global model [*Chassignet and Marshall*, 2008]. Furthermore, the latitude of the separation of the EAC pathways is variable and has a significant impact on local climate, ecosystems, and cross-shelf dynamics like upwelling at nearby regions [e.g., *Roughan et al*., 2003; *Hobday and Hartmann*, 2006; *Schaeffer et al*., 2013].

This paper is one of the first attempts to investigate the upstream control and the potential vorticity structure of the water masses that separate at the bifurcation of the EAC from a Lagrangian perspective. Previous studies show that the Lagrangian approach is suitable in this region [e.g., *Van Sebille et al*., 2012; *Cetina-Heredia et al*., 2014]. An additional advantage of using a Lagrangian perspective is that, unlike an Eulerian approach, the direct connectivity between sources and sinks of water masses can be studied.

In this study, we use numerical Lagrangian float trajectories advected within a 1/4° global ocean sea-ice model, which allows us to make a distinction between water flowing eastward following the Tasman Front and water continuing southward in eddies forming the EAC extension. This will give an idea of where and how the bifurcation of water particles in the EAC is determined. We will investigate the upstream control of the fate of the water by studying the distribution of the particles upstream and downstream of the separation latitude. Furthermore, anomalies and changes in the in situ potential vorticity structure for the two pathways upstream and around the separation latitude are studied to show which components of the potential vorticity determine the structure of the PV anomaly and how this relates to the bifurcation of the two pathways.

The next section presents a brief description of the ocean model used, the setup of the Lagrangian experiment, and how the distinction between the pathways is made. Additionally, the calculations made to

analyze the potential vorticity of the pathways are discussed. Section 3 will provide a brief validation of the ocean model, followed by the analysis of the trajectories of interest in section 4, including an examination of the potential vorticity changes at the region of the EAC separation, followed by a general discussion and summary of our main results in section 5.

2. Data and Method

2.1. The Ocean Circulation Model

To investigate the EAC separation we have used 5 day averages of the Geophysical Fluid Dynamics Laboratory (GFDL) Modular Ocean Model (MOM025), which is sufficient to capture the progression and retraction of the EAC separation latitude and the temporal variability caused by the eddies [*Bowen et al.*, 2005; *Cetina-Heredia et al.*, 2014; *Qin et al.*, 2014]. GFDL-MOM025 is based on the ocean component of the GFDL CM2.4 and CM2.5 coupled climate models [*Farneti et al.*, 2010; *Delworth et al.*, 2012]. GFDL-MOM025 is a global ocean-sea-ice model with 50 levels in the vertical (with a 10 m resolution in the upper 100 m up to a 200 m resolution in the bottom layers) and a 1/4° eddy-permitting horizontal resolution with no-slip boundary conditions at lateral sidewalls, coupled to the GFDL Sea Ice Simulator dynamic/thermodynamic sea-ice model. The atmospheric state is prescribed and converted to ocean surface fluxes by bulk formulae. There are no air-sea feedbacks and for the analysis a "normal year" atmospheric forcing is used constructed from version 2 of the Coordinated Ocean-ice Reference Experiments Normal Year Forcing (CORE-NYF) reanalysis data [*Griffies et al.*, 2009; *Large and Yeager*, 2009]. CORE-NYF consists of a climatological mean atmospheric state at 6 h intervals for 1 year [*Griffies et al.*, 2009]. Since the model is run using the same seasonal forcing every year, there is no interannual variability present in the forcing fields and all variability seen in the model output on time scales larger than a year can therefore only be caused by internal ocean processes. Using normal year forcing instead of interannual forcing is advantageous to our study, since we are only interested in internal ocean dynamics.

The ocean components of the next generation of climate models, which will form the bulk of CMIP6, will likely be eddy-permitting at a 1/4°–1/3° horizontal resolution. This means that even though a 1/4° model might not capture all dynamical aspects by underestimating the eddy activity, it is still important to understand the physical mechanisms that are present in ocean models at this resolution.

2.2. Particle Tracking

Lagrangian particles are released every 5 days for 10 years upstream of the EAC separation and advected forward in time with a time step of 1 h within the 5 day averages of the 3-D velocity field output of the ocean model, using the Connectivity Modeling System (CMS v1.1) [*Paris et al.*, 2013]. The CMS model uses a tricubic interpolation spatially and a fourth-order Runge Kutta stepping scheme in time. No horizontal or vertical diffusivity is added to the particles, so the particle motion is purely advective. The particles are released at a zonal transect at 26°S between 154°E and 155.5°E (0.25° apart) within the top 1000 m (10 m apart). Since particles flowing at depths deeper than 1000 m are mainly recirculated in the Tasman Sea [*Ridgway and Dunn*, 2003], they are not considered as part of the two pathways of interest. Particles reaching the east coast of Tasmania, between 42.5°S and 41.5°S and between 148°E and 150°E, are defined here to form the extension of the EAC (Figure 1). Particles flowing through a box north of New Zealand, between 31°S and 36°S and between 173.5°E and 175°E, are defined here as taking the Tasman Front pathway. For this study, the boxes are chosen such that a large number of particles is captured and that most particles crossing the boxes eventually leave the Tasman Sea and are not recirculated. This way, a total of 1.4×10^5 particles that follow the Extension of the EAC and 1.1×10^5 particles that follow the Tasman Front are advected for up to 4 years, to make sure that the majority of the particles following the extension of the EAC had enough time to pass the southern tip of Tasmania [*Van Sebille et al.*, 2012].

2.3. Potential Vorticity Along the Trajectories

The potential vorticity structure of the EAC region is a useful diagnostic to investigate the importance of relative vorticity, stratification, friction, and diabatic processes. The vertical component of the Ertel potential vorticity (PV) is given by

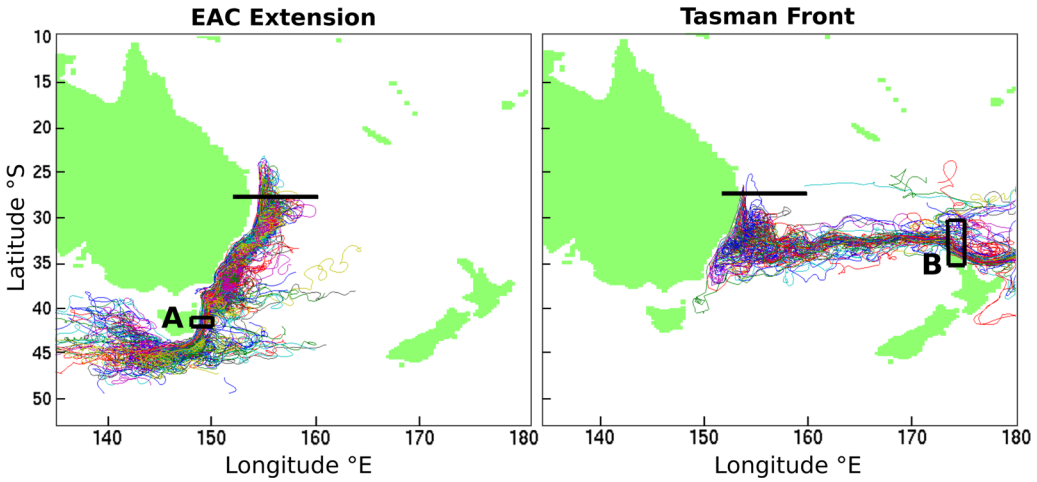

Figure 1. Random subset of 80 particles advected in the ocean model following (left) the pathway of the extension of the EAC and (right) the pathway of the Tasman Front, following their release at 27°S. Particles traveling through box A (41.5°S–42.5°S and 148°E–150°E) are selected to form the extension of the EAC. Particles traveling through box B (31°S–36°S and 173.5°E–175°E) form the pathway of the Tasman Front. The black line shows the transect at 28°S which is located upstream of the separation latitude. Coloring is random.

$$q = -\frac{f+\zeta}{\rho_{ref}}\frac{\partial \rho}{\partial z}, \tag{1}$$

where f is the planetary vorticity, ζ the relative vorticity, ρ_{ref} the reference density of 1035 kg/m^3, and ρ the in situ density, where $\partial\rho/\partial z$ is a measure of stratification [e.g., *Dijkstra*, 2008]. If the Richardson number ($\mathrm{Ri} = N^2/|\partial \mathbf{u}_h/\partial z|^2$, where N^2 is the squared buoyancy frequency and $\mathbf{u}_h$ the horizontal velocity) of the flow is large, and vertical shear and horizontal density gradients are small, q is conserved when following a water parcel in the absence of diabatic and frictional processes. The decomposition of the two pathways of interest allows us to investigate differences in anomalies in potential vorticity around and upstream of the separation latitude. Looking at anomalies in potential vorticity and its constituents (relative vorticity and stratification) will show which component is controlling the structure of the PV anomaly and how this relates to the bifurcation of the two pathways. The same approach will be used to look at changes in the potential vorticity terms along the trajectories to see if and where these terms are conserved.

For all particles, and for every 5 days along their trajectories, the in situ potential vorticity (q) at their longitude, latitude, and depth is calculated. First, q, ζ, and $\partial\rho/\partial z$ are calculated from the velocity and density fields from the ocean model by central differencing. Then, the fields are linearly interpolated over a 0.1° lon $\times$ 0.1° lat $\times$ 10 m depth bin to be able to interpolate the obtained values onto the location and time of the particles using a nearest neighbors search.

The value of stratification is negative at all times, since the water columns in the ocean model used are kept statically stable by parameterized convection. The planetary vorticity is negative in the southern hemisphere and the Rossby number ($Ro = |\zeta/f|$) calculated from the MOM025 fields in this region reaches values of 0.2, indicating that planetary vorticity is larger in magnitude than the relative vorticity. The minus sign in equation (1) is chosen such that the potential vorticity will be negative in most locations in order to match other definitions of potential vorticity [*Holmes et al.*, 2014].

3. Validation of the Modular Ocean Model Circulation

To validate the results of the model, a comparison is made between the model output and observed sea surface height (SSH) from the Archiving Validation and Interpretation of Satellite Oceanographic data (AVISO) by investigating the mean, the variability, the location of EAC separation, and the volume transport. The AVISO product used provides Mean Absolute Dynamic Topography (DT-MADT), Delayed Time mode, on a 0.25° by 0.25° Cartesian grid with a 7 day temporal resolution from 1992 to 2010.

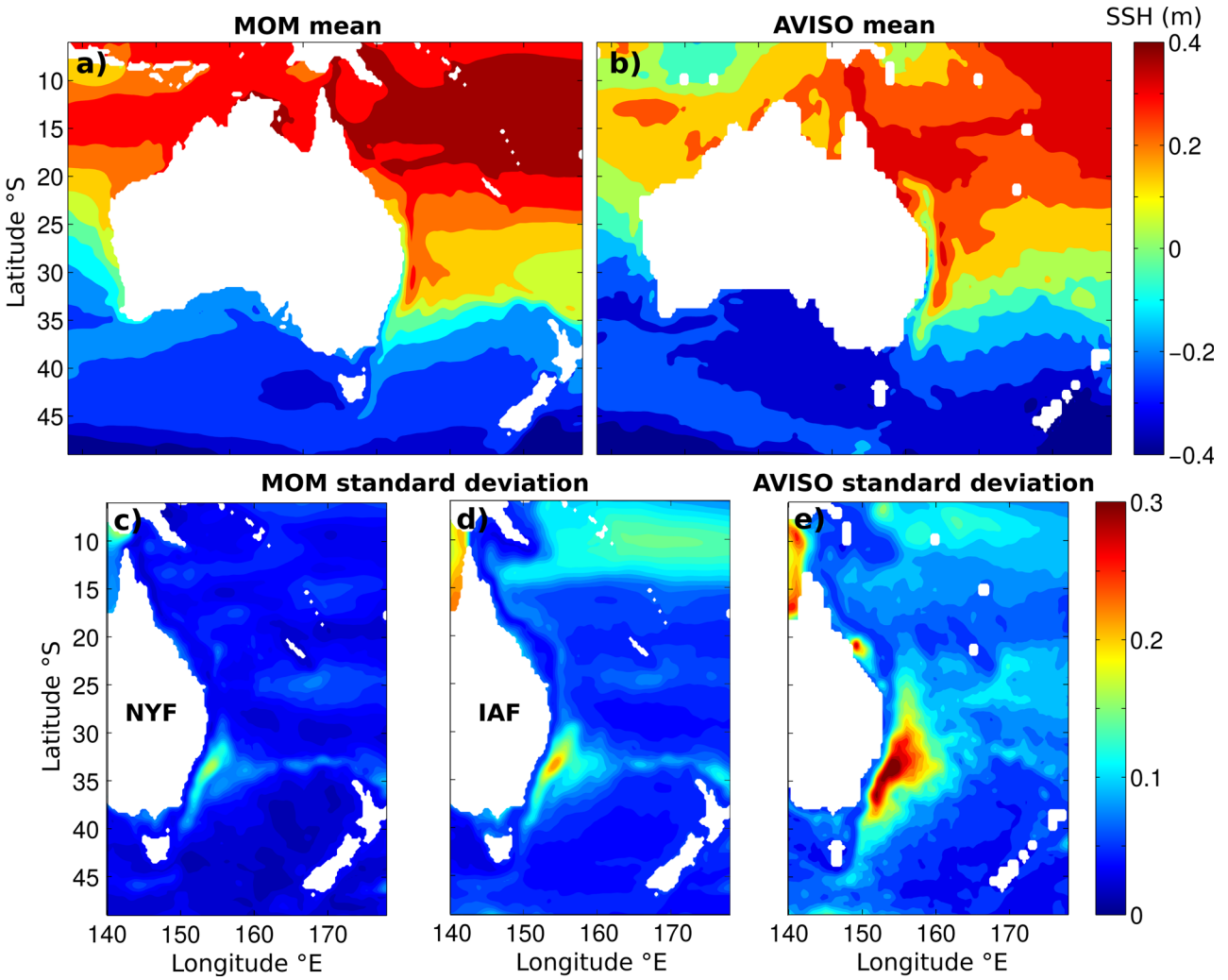

Figure 2. (a, c, d) Mean and standard deviation (in m) of the Sea Surface Height (SSH) for the 1/4° MOM025 model output and (b, e) the mean absolute dynamic topography from AVISO satellite altimetry. Figures 2a and 2c have normal year forcing and Figure 2d has interannual forcing. The model output with interannual atmospheric forcing accounts for 30% of the missing variability.

3.1. Mean and Variability of the Sea Surface Height

The mean and the standard deviation of the sea surface height are calculated from the model and AVISO altimetry data (Figure 2) over the entire length of the data sets (19 years for AVISO, 40 years for the model). Since interannual variability is low in the model, the number of years chosen to average over will not change the mean state found. The observed SSH is however averaged over the entire data set to minimize influences from interannual variability on the mean state. The mean of the SSH is in good agreement with observations and the pathway of the EAC is clearly visible (Figures 2a and 2b). However, the standard deviation of SSH in the model, which is a measure of the variability or eddy activity, shows only half the magnitude of the variability seen in AVISO (Figures 2c and 2e). The Tasman Front in the model seems to have a very narrow band of variability extending eastward at approximately 33°S, whereas in the satellite observations this pathway is not as clearly visible and seems to be more broad.

Van Sebille et al. [2012] studied the same region using the Ocean Forecast for the Earth Simulator (OFES), which is based on an older version of the Modular Ocean Model (MOM3), but has a 1/10° horizontal resolution. They found a good agreement in SSH variability between AVISO and their model output, suggesting that the lower resolution of MOM025 leads to reduced SSH variability. Furthermore, part of the missing variability in the region of the EAC separation can be explained by the missing interannual atmospheric variability. The same model forced by interannual forcing shows an increase of ∼30% in the variability (Figure 2d).

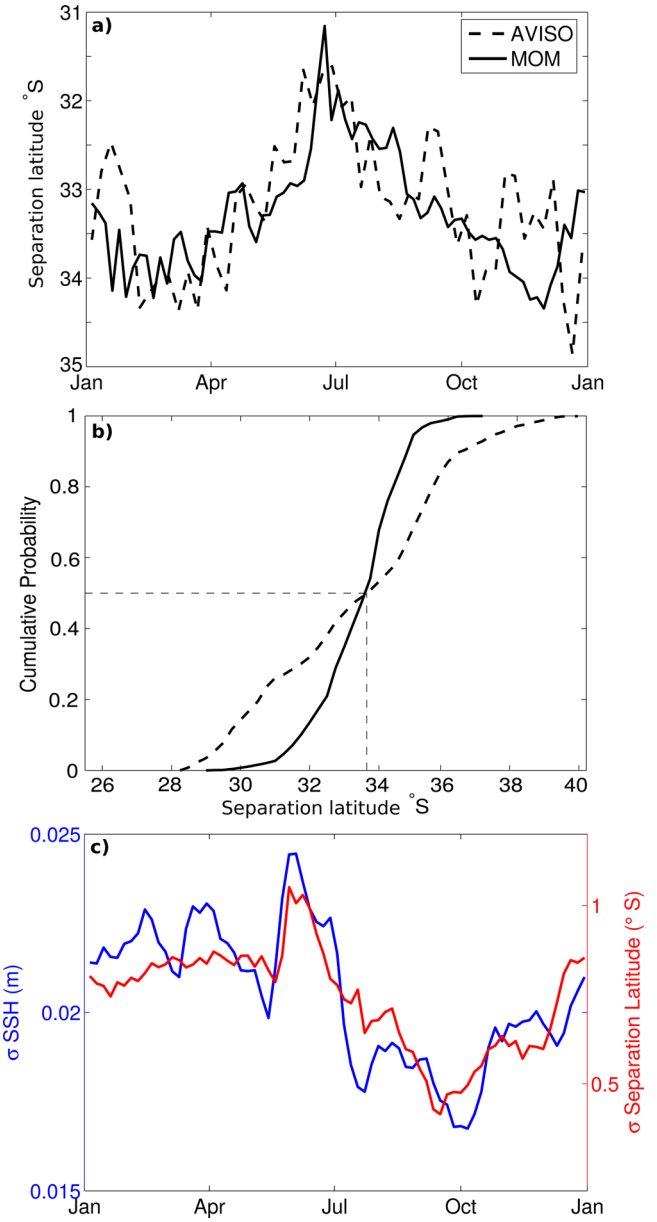

Figure 3. (a) Mean separation latitude and (b) cumulative distribution function of the EAC separation latitude time series computed from MOM025 (solid line) and the AVISO satellite altimetry data set (dashed line). The length of the time series used is 40 years for MOM025 and 19 years for AVISO. The median separation latitude in both MOM025 and AVISO is 33.6°S. (c) Time series of the standard deviation of sea surface height (blue) and the separation latitude (red) of the ocean model, determined using a 55 day running mean. The average over 15 years is shown. Taking an average over a different number of years does not change the location of the maximum and minimum, since the years are very similar due to the normal year forcing used in the model. Additionally, the standard deviation of the sea surface height is averaged over the area between 20°S and 45°S and between 150°E and 160°E.

3.2. Separation Latitude of the EAC

In order to validate the model further, the time series of the EAC separation latitude is used to compare the location and variability of separation between the model and AVISO. The method of estimating the latitude at which the EAC veers eastward is based on the method described by *Cetina-Heredia et al.* [2014], where SSH contours are used to find the veering point of the main current. The core of the EAC is found upstream of the separation by selecting the maximum southward geostrophic surface velocity at a 28°S transect, calculated from the SSH field. Then, the SSH isoline coinciding with the location of the maximum velocity is followed and the first location at which the isoline turns more than 30° eastward of south is recorded as the separation latitude. This method has been shown to be appropriately sensitive to both eddy detachment and reattachment, which strongly influence the location of separation [*Cetina-Heredia et al.*, 2014]. The chosen threshold of 30° might result in values of the separation latitude that are slightly further to the south than in situ observations indicate. By the time the SSH contour has turned 30°, its actual separation from the coast has already taken place further north. However, since we use the same method for the model data and the observations from satellite altimetry, this is still a good method to validate the model's representation of the separation.

The temporal average of the separation latitude over the years of data available shows a clear dependence on the seasonal cycle (Figure 3a). The standard deviation in the separation latitude of the model is 0.5°–1° (Figure 3c), while the standard deviation in the observations is much larger (Figure 3b), so this seasonal cycle will not be very clear in most years and only shows up in the climatology. However, the standard error in the mean for both data sets is of order 0.1°; therefore, the seasonal cycle observed is statistically significant. In both the model and the observations the most northern separation latitude is reached in July, whereas the most southern latitudes are reached between December and April. This is in agreement with the in situ observed movement of the steric height field throughout the year with a maximum southward extension of the EAC in summer [*Ridgway and*

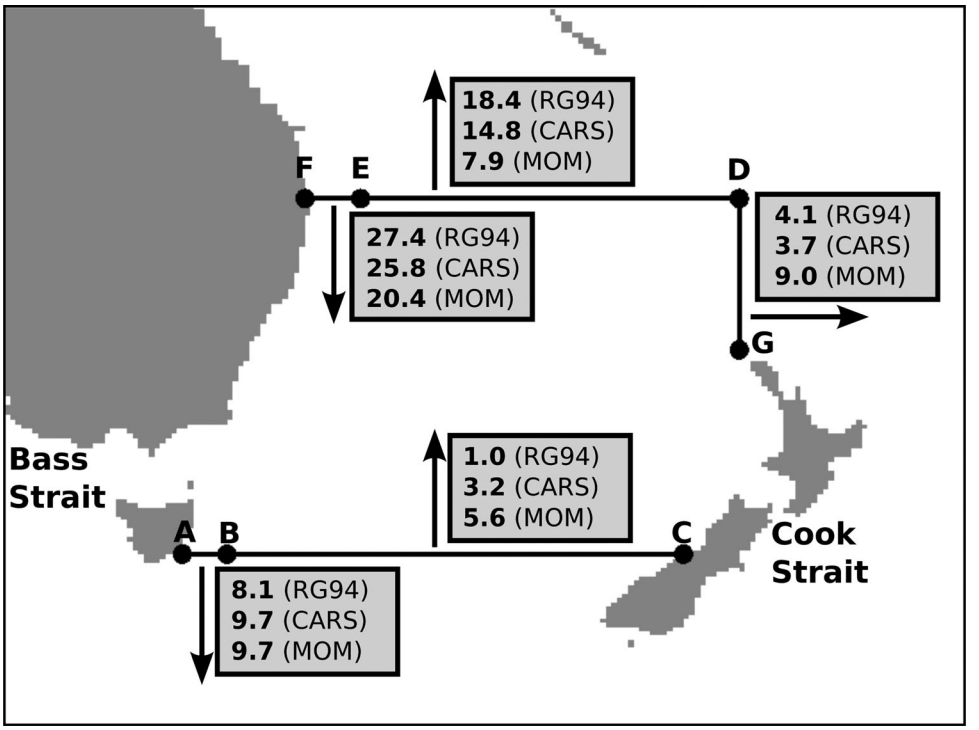

Figure 4. Mean net volume transport into and out of the Tasman Sea over the 0–2000 m depth range. The numbers in the boxes indicate the transport (in Sv) in the direction of the corresponding arrow. The transports calculated by the model (MOM025) are compared to estimates from observations, *Ridgway and Godfrey* [1994] (RG94) and CARS, derived by *Oliver and Holbrook* [2014]. The sections are defined by the following locations: A (148°E, 43°S), B (150°E, 43°S), C (170.5°E, 43°S), D (173°E, 28°S), E (156°E, 28°S), F (153.5°E, 28°S), and G (173°E, 34.4°S).

Godfrey, 1997]. Furthermore, the time series show a steeper slope of the EAC separation retraction northward compared to the progression of the separation southward. This skewness could be explained by the observed higher eddy kinetic energy in late summer and autumn in this region, implying more eddy-shedding events [*Qiu and Chen*, 2004; *Cetina-Heredia et al.*, 2014] (Figure 3c).

The cumulative probability of the time series obtained shows the underlying distribution of the separation latitude (Figure 3b). Per degree of latitude at which the maximum southward geostrophic velocity is selected, the median separation latitude can shift southward or northward by 0.3°–0.4°. However, the shape of the cumulative probability function stays the same. Therefore, it is possible to use the method of determining the separation latitude to compare the underlying distribution in MOM025 and AVISO.

From the cumulative probability of the time series, we can conclude that the median of the separation latitude in the model agrees very well with the observations. The distribution of the modeled separation latitude is however much narrower, consistent with the model's underestimation of SSH variability. This, again, can be explained by the relatively low horizontal resolution in the ocean model and the effect of the missing atmospheric variability in the forcing. The difference of the recorded separation latitude between the model and the AVISO data are slightly larger at the southern end of the distribution than at the northern end of the distribution. It is likely that this skewness is caused by the observed trend in the EAC separation latitude, where the current is found to separate more often at the southernmost latitudes in recent years [*Cetina-Heredia et al.*, 2014].

3.3. Volume Transport in the Tasman Sea

The Eulerian volume transport in the Tasman Sea is calculated for different sections by multiplying the normal velocity component with the grid area and integrating over the upper 2000 m of the water column. The transport is compared to estimates derived from the mean dynamic topography relative to 2000 m from CSIRO Atlas of Regional Seas (CARS) climatology (as in *Oliver and Holbrook* [2014], *Ridgway et al.* [2002], *Dunn and Ridgway* [2002], and *Condie and Dunn* [2006]) and estimates given by *Ridgway and Godfrey*

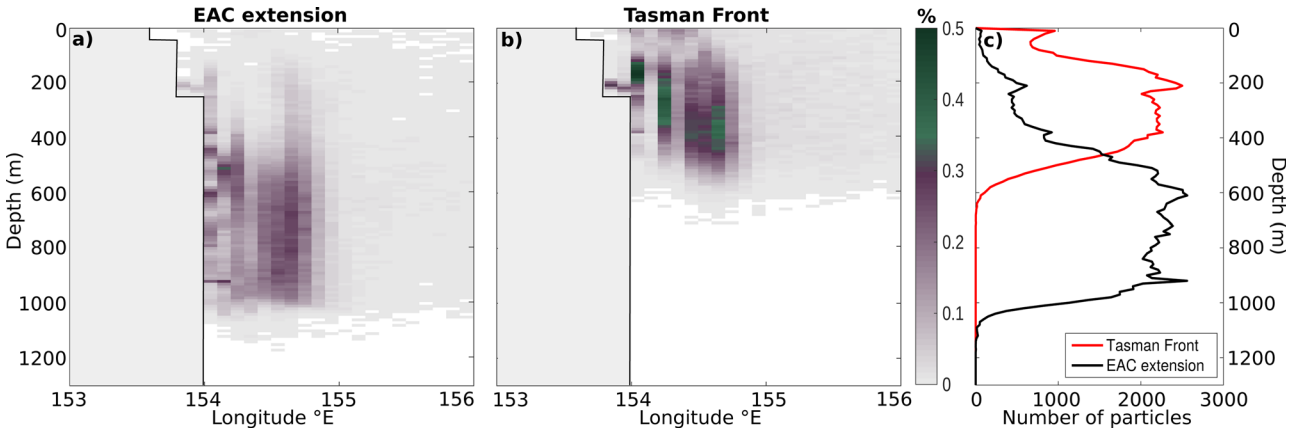

Figure 5. Depth profile at 28°S (transect shown in Figure 1) upstream of the separation latitude of the particle density (a) for particles following the extension of the EAC and (b) for particles following the Tasman Front. The gray shading on the left side of the figures represents the model bottom topography at this latitude. (c) The number of particles with depth integrated over longitude for both pathways gives the partition depth of 460 m.

[1994] based on observations of 6000 hydrological stations. The different segments are indicated by letters chosen to match *Oliver and Holbrook* [2014] (Figure 4).

At the northern boundary of the Tasman Sea, the inflow from the EAC (EF, Figure 4) and the flow northward across 28°S (DE) in the model are both lower than the volume transport estimated from observations, indicating that the EAC strength is weaker in the model than in observations. The transport across the meridional section at 173°E (DG) is however overestimated. Similar to the results from the standard deviation of the SSH and the findings of *Oliver and Holbrook* [2014], this suggests that the model predicts a more focused eastward flow along the Tasman Front than observations do. At the southern boundary of the domain, the model estimates for the narrow flow along Tasmania from the EAC extension (AB) are similar to the observations. The northward transport is slightly overestimated (BC).

The net transport out of the domain bounded by A-F of the ocean model is 0.6 Sv compared to −0.8 Sv estimated from CARS and 2.2 Sv estimated by *Ridgway and Godfrey* [1994]. The imbalance in the model can be explained by leakage through the Cook and Bass straits and the transport taking place at depths below 2000 m. The imbalances for the observations are larger and are of opposite signs, indicating that the observed values are uncertain as well, which is partly caused by the highly variable transport in this region.

The Lagrangian particles advected in the ocean model are used to provide a second method to estimate transport, although only for the upper 1000 m where particles were seeded. Every particle is tagged with its transport at the time of release by multiplying the southward velocity with the area (0.25° lon × 10 m thickness). From this an estimate can be made for the proportion of water that originates from the EAC and follows the Tasman Front or follows the extension of the EAC. The results show that a large part (∼40%) of the transport from the EAC is following the Tasman Front pathway and only ∼14% of the total transport is following the extension of the EAC. The remainder of the transport in the EAC is carried by particles that recirculate within the Tasman Sea and do not reach Tasmania or New Zealand (Figure 1). This is in agreement with previous estimates that show a 1:3 ratio between transport in the extension of the EAC and transport in the Tasman Front [*Hill et al.*, 2011].

We conclude that although the model does not reproduce all features of the East Australian Current region as seen in observations, it shows sufficient skill to assess the two pathways after the EAC separates from the coast.

4. Results

4.1. Upstream Control by Particle Distribution

The depth profile of the particle density distribution upstream of the separation latitude at 28°S is shown in Figure 5 for particles traveling southward as part of the EAC extension and for particles traveling eastward along the Tasman Front. A clear distinction in the distribution of the particles with depth between the two

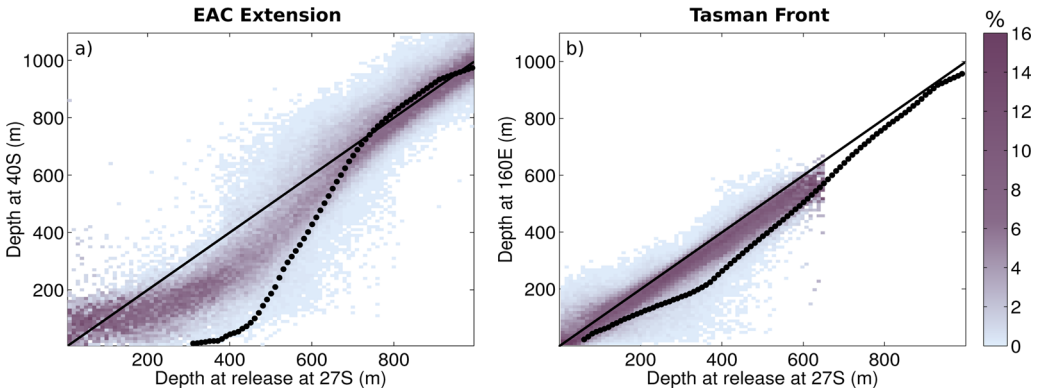

Figure 6. The distribution of particle depths at transects after the separation (vertical axis) as a function of depth from which the particle originated at 27°S (horizontal axis). The transects after the separation are chosen at 42°S and 160°E for the extension of the EAC and the Tasman Front, respectively. The black solid line represents $y = x$; high percentages coinciding with this line indicate that particles have no net change in depth. The distribution shown is calculated per depth interval of 10 m thickness separately. The black dotted line represents the mean change in depth of isopycnals corresponding to the chosen transects. Note that to highlight the behavior of the particles of each layer, even those where there is relatively low transport, the percentages are normalized by the total number of particles in each release layer.

pathways can be observed, but the zonal distribution is very similar. 85% of the particles following the extension of the EAC originate from the deeper part of the EAC flow below a depth of 460 m (the cutoff below 1000 m is due to the initial particle seeding). The particles that form part of the Tasman Front, however, originate from the upper part of the EAC, where 90% originate from the layer between the surface and 460 m depth. Shifting the chosen transect southward or northward upstream of the separation location does not change this distribution. There are no particles in this simulation that originate from a depth deeper than 700 m ending up north of New Zealand while following the Tasman Front, in agreement with the observed values by *Sutton and Bowen* [2014]. This indicates that whether a particle follows the Tasman Front or the EAC extension (the "fate" of a particle) is to some extent already determined before the EAC bifurcates.

The change in depth from before the bifurcation, at 27°S, to after the bifurcation, at 40°S and 160°E for the extension of the EAC and the Tasman Front particles, respectively, is shown in Figure 6. Of the particles following the extension of the EAC, 32% originate from 200 to 600 m depth and seem to be advected upward in the water column by up to 200 m (Figure 6a). Note that we are only considering the initial and final depths; particles may have additional vertical excursions in between. Below 600 m the particles do not change their depth significantly. The particles that follow the Tasman front show a mean shift upward of only 50 m (Figure 6b) and their distribution in the water column has a smaller extent than the particles that follow the extension of the EAC.

This behavior can be compared to the outcropping of time-mean isopycnals. We note the presence of isopycnal outcropping in the top 300 m from 27°S to 40°S (dotted line Figure 6a). From 300 to 700 m depth, the isopycnals show an upward slope which is strongest at shallower depths, and below 700 m their depth does not change. The behavior of the isopycnals in this region is mainly explained by the strong gradient in surface density over the transects chosen. Comparing the depth of the isopycnals between the transects at 27°S and 160°E along the Tasman Front, the isopycnals are slightly pushed up (dotted line in Figure 6b), which is explained by the fact that the transect at 160°E lies poleward of 27°S, at around 34°S where the mean density is higher.

At face value, the results seem to indicate that particles following the extension of the EAC only partly follow isopycnals, as seen in the differences between the distribution of particle depth change and the curve of the time mean depth change of the isopycnals (Figure 6a). While this could indicate that the particles experience strong diapycnal downwelling, it could also be because the mean density field is not a good representation of the density field seen by the particles that follow the extension of the EAC. In this latter explanation, a possible hypothesis is that a large part of these particles might be trapped in warm-core anticyclonic eddies and therefore experience a lower density than the mean flow around them at the transect

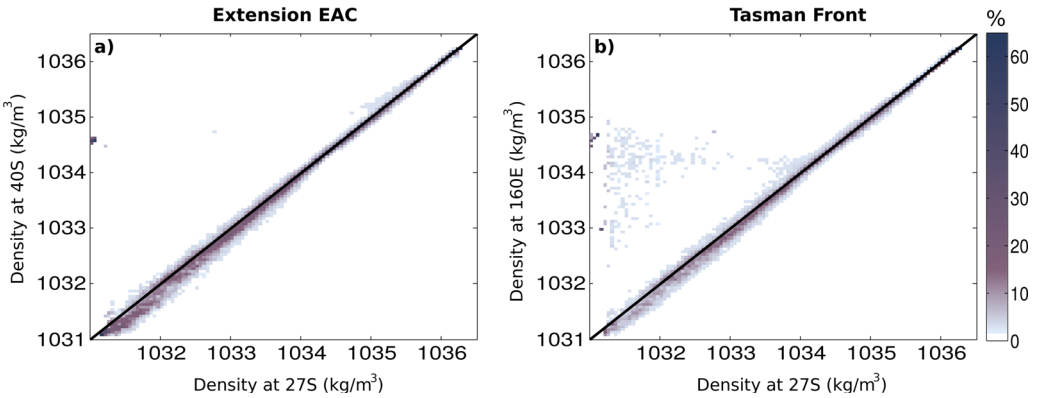

Figure 7. The distribution of particle potential density at transects after the separation (vertical axis) as a function of the original potential density of the particle at 27°S (horizontal axis). The transects after the separation are chosen at 42°S and 160°E for the extension of the EAC and the Tasman Front, respectively. The black solid line represents $y = x$; high percentages coinciding with this line indicate that particles have not changed their density. The distribution shown is calculated separately for each density interval of 0.05 kg/m^3 at 27°S.

at 40°S. The result would then be that these particles do follow isopycnals, or at least experience a smaller upward advection than the mean density surfaces suggest.

To investigate whether the displacement of the particles is due to vertical movement of isopycnals or due to mixing across isopycnals, the change of the particle's potential density between the transects (27°S–40°S and 27°–160°E) is calculated (Figure 7). For the particles following the EAC extension and the Tasman Front, 80 and 67% (respectively) have a density change of less than 0.2 kg/m^3. From this, it is clear that particles tend to follow isopycnals reasonably well. Therefore, the most likely hypothesis for the discrepancy seen in Figure 6a between the distribution of the particles' change in depth from 27°S to 40°S and the curve of the change of depth of the isopycnals is that most of the particles in the upper 600 m travel southward within warm anticyclonic eddies, and so their upward displacement is less than that of the mean isopycnals.

4.2. Control by Eddy Activity

The number of particles taking each route at the bifurcation varies with time. For the subset of particles that follow the EAC extension the largest fraction crosses the 28°S transect in September (14.5%, Figure 8a) and the smallest fraction crosses the transect in May (3.8%), where the percentages are normalized for each pathway individually. There is some variability in the subset of the particles that follow the Tasman Front, but it does not show a strong seasonal dependence. Although previous studies find an anticorrelation between Tasman Front transport and the transport in the EAC extension [e.g., *Sloyan and O'Kane*, 2015], our results show that less water ending up in the extension of the EAC does not necessarily lead to more water following the Tasman Front or vice versa. This is supported by the findings of the previous section that the water masses of the two pathways are originating from different depths in the EAC.

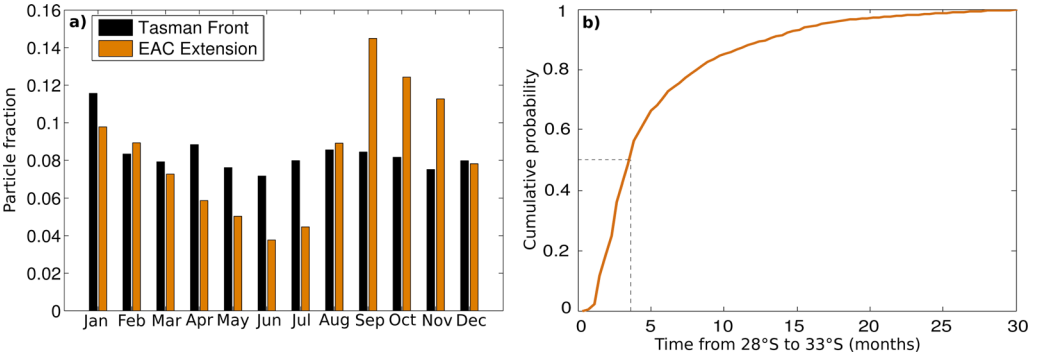

Figure 8. (a) Histogram of the time in the year when a particle crosses the transect at 28°S. The vertical axis shows the ratio between the number of particles crossing the transect in a given month to the total number of particles following the specified pathway. The particle fraction is normalized for each pathway individually. (b) The cumulative probability of the transit time from 28°S to 33°S for the particles following the EAC Extension crossing 28°S in September.

The transit time from the transect at 28°S to the median separation latitude of 33°S is shown, in a cumulative sense, in Figure 8b for the particles that cross 28°S in September. Half of the particles arrive at the separation at 33°S within 4 months (i.e., before January), but the transit time distribution ranges from a minimum of 22 days to more than a year. This suggests that a large fraction of particles are trapped in eddies north of the mean separation latitude of 33°S. Furthermore, investigation of the particle trajectories reveals that some particles take a long detour away from the coast and the EAC before reaching 33°S, which are not shown in Figure 1.

The strong seasonal variability seen in the number of particles following the extension of the EAC is likely related to the strong seasonal variability observed in the EAC separation latitude (Figure 3a) and the eddy activity (Figure 3c). In western boundary current regions the standard deviation in sea level height is mostly caused by mesoscale eddy variability [*Zlotnicki et al*., 1989; *Thompson and Demirov*, 2006] and can therefore be used as an indicator for eddy activity.

The seasonally averaged eddy activity and the variability seen in the seasonally averaged separation latitude are highly correlated (Figure 3c, $R = 0.87$). As discussed in section 3.2, this can be explained by the eddy-shedding process, where higher eddy activity is caused by more eddy shedding and therefore larger variability in the separation latitude. The variability is high from January through to June, while the separation latitude moves equatorward from its most southern excursion (Figure 3a). The maximum variability seems to be reached in June, which is a few weeks before the most northern separation latitude is reached (Figure 3). Then, the variability quickly drops down to a minimum in October and starts slowly increasing from October onward. Combining this result with the transit time from 28°S to 33°S (Figure 8b), it seems that the number of particles ending up in the extension of the EAC is dependent on the eddy activity and where the separation takes place. The results suggest that the largest transport across the separation latitude takes place around January, when the eddy activity is high and the EAC separates at the southern end of its range.

4.3. Relation Between Particle Path and Potential Vorticity

The future pathway of the particles in the EAC seems to be mostly controlled by the depth of the particles upstream of the separation latitude (section 4.1). However, as seen in Figure 5, there is an overlapping region between the surface and a depth of approximately 600 m where the particles can either follow the extension of the EAC or the Tasman Front. Using a potential vorticity analysis of the overlapping region will highlight whether particles experience different potential vorticity, relative vorticity, and stratification when they follow different pathways and in which region these differences are most pronounced. This section will focus on the evolution of vorticity for both particle pathways in the overlapping region at about 400 m depth, where the overlap between the number of particles of both pathways is maximal.

Anomalies of potential vorticity, stratification, and relative vorticity are calculated for both pathways (Figure 9). Particles are selected when traveling through one of the 0.1° lon $\times$ 0.1° lat grid boxes in a layer between 350 and 450 m depth, where the particles of both pathways are approximately evenly distributed. The values shown are averages over 100 randomly selected particles at that grid point, to be sure that the results are not biased by the number of particles present. All locations containing less than 100 particles are not shown. To be able to understand the resulting anomalies, the time mean of the potential vorticity, relative vorticity, and stratification from the model are shown as well (Figures 9a, 9d, and 9g).

The resulting anomalies in the potential vorticity terms are 5–10 times smaller than the values for the mean potential vorticity and $\partial\rho/\partial z$ and roughly half the values of the mean relative vorticity. From 33°S to 38°S close to the coastline, the 100 particles selected per grid box show large deviations in the potential vorticity terms from the mean of similar magnitude to the anomaly itself at that location. This indicates that there is a high variability of vorticity in this region and therefore the anomaly close to the coast south of 33°S should be interpreted carefully.

There is a clear difference between the two pathways in the anomalies for all the vorticity terms upstream of and around the separation latitude (34°S). The potential vorticity anomaly is strongly positive at the eastern side of the particle trajectories following the extension of the EAC (Figure 9b). In the same region, the particles following the Tasman Front show a negative anomaly in potential vorticity (Figure 9c). For both pathways, this region falls outside the regions with a large spread in potential vorticity, and the difference

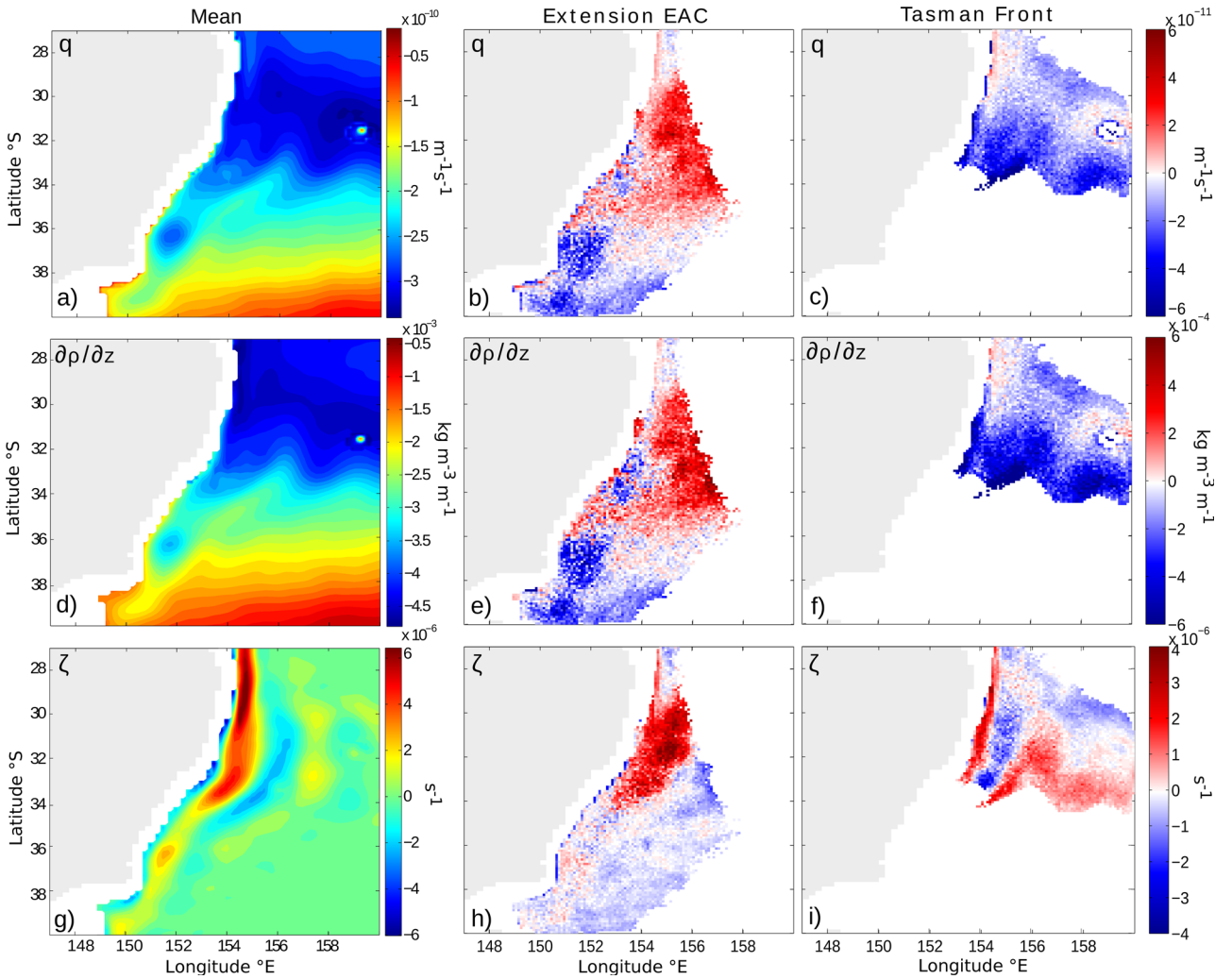

Figure 9. The time mean of potential vorticity (q), stratification ($\partial\rho/\partial z$), and relative vorticity (ζ) (left column) averaged over 14 years of model output, corresponding to the years the particles are advected in, and averaged over the layer between 350 and 450 m depth. (middle column) The anomaly for q, $\partial\rho/\partial z$, and ζ relative to the 15 year average of these terms for particles following the extension of the EAC and right column: particles following the Tasman Front. The anomalies are calculated from the mean of a random sample of 100 particles per grid box located between 350 and 450 m depth.

observed between the anomalies in q of particles following the extension of the EAC and particles following the Tasman Front is therefore robust. These patterns are mainly caused by the anomalies seen in the stratification (Figures 9e and 9f), which indicates that layer thickness variations are dominating the structure of potential vorticity.

Between 30°S and 32°S, particles following the EAC extension show a positive $\partial\rho/\partial z$ anomaly, indicating a decrease in stratification from the mean (Figure 9e). To explain this, it is important to know where the pycnocline is located and how eddies influence the density profile in this region. In the mean state, the pycnocline is located at 400 m depth north of 32°S. From 32°S to 34°S a sharp decrease in depth of the pycnocline is observed, coinciding with the outcropping of warm Coral Sea water. Since our chosen layer is located at the pycnocline depth in the northern region of our domain, upward or downward shifting of the pycnocline would both cause a reduction in stratification. The same region shows a positive anomaly in relative vorticity (Figure 9h), indicating more anticyclonic behavior compared to the mean. Anticyclonic eddies have the tendency to push isopycnals, and therefore the pycnocline, down [e.g., *Cushman-Roisin and Beckers*, 2011]. Apparently, particles flowing along the EAC extension experience more anticyclonic behavior, which causes a reduction in the stratification and potential vorticity around 32°S, consistent with their transport in anticyclonic eddies, as inferred also from Figures 6 and 7.

The particles that follow the Tasman Front show a negative anomaly in $\partial\rho/\partial z$, indicating an increase in stratification with respect to the mean state. The negative signature is even stronger farther south. It is possible that this behavior is caused by a horizontal shift of the outcropping region of the pycnocline. Shifting this region to the south would bring the more stratified water of the pycnocline to a region of less stratified water at the depth of 400 m, explaining the observed anomaly in stratification. This is an indication that particles following the Tasman Front are controlled by the strong horizontal gradient in density seen in the upper 400 m around 33°S, caused by the outcropping of isopycnals. Particles following the Tasman Front can only reach higher latitudes when this barrier is pushed southward.

The anomaly in relative vorticity for particles following the Tasman Front shows a positive anomaly close to the coast following the southern boundary of the particle trajectories, but a slightly negative anomaly away from the coastline (Figure 9i). Interestingly, the mean state of relative vorticity shows a similar pattern (but opposite sign) with negative (cyclonic) regions and positive (anticyclonic) regions further offshore (Figure 9g). This could indicate that particles following the Tasman Front experience a reduction in both anticyclonic and cyclonic behavior compared to the mean. The reduction can be caused by less eddy activity or by a weakening or retraction of the flow.

Combining the results of the anomalies seen in the potential vorticity terms it seems that anticyclonic eddies play a crucial role in pushing isopycnals down and transporting particles southward across the barrier of strong horizontal density gradients.

We have seen that layer thickness variations are dominating the structure of potential vorticity. However, this does not necessarily imply that potential vorticity changes along particle trajectories are dominated by stratification changes. Since particles to first order follow contours of constant isopycnal spacing, the contribution to Lagrangian potential vorticity change from stratification is reduced. Therefore, we also compute the material derivative of potential vorticity, stratification, and relative vorticity along the trajectory of the particles and visualize these in the same way as the anomalies of these terms (Figure 10). The results show the change along a trajectory over 5 days. The standard error of the mean is at least 1 order of magnitude smaller than the calculated values, indicating that the means shown are statistically different from zero.

The results for the particles following the extension of the EAC and the particles following the Tasman Front show a similar pattern. If there were no Reynolds terms, this would indicate that the initial PV difference between the trajectories would be preserved, because particles would experience identical changes traveling downstream. However, as seen in Figures 9b and 9c a difference in the potential vorticity does develop between the trajectories around 29°S–32°S. This indicates that the mean streamlines differ and/or the Reynolds term is significant, i.e., the instantaneous particle paths differ significantly from the mean. It is clear that potential vorticity is relatively well conserved on the offshore side of the domain. However, close to the coast changes in potential vorticity are sigificant where an $O(1)$ change of PV can take place within 50 days. It is possible that friction causes the PV conservation to break down in this region.

North of 31°S the potential vorticity is decreasing downstream at the onshore side of the current and increasing downstream at the offshore side (Figures 10a and 10b). Comparing this region to the patterns seen for the Lagrangian change in $\partial\rho/\partial z$ (Figures 10c and 10d) and relative vorticity (Figures 10e and 10f), the changes in PV are due to changes in relative vorticity, rather than changes in stratification. The relative vorticity shows a decrease in ζ at the cyclonic side and an increase in ζ at the anticyclonic side, implying that both cyclonic and anticyclonic behavior is increasing downstream. This is in agreement with downstream acceleration prior to separation in previous studies on western boundary current dynamics with no-slip lateral boundary conditions [*Kiss*, 2002, 2010].

The striped pattern seen in the Lagrangian rate of change in relative vorticity at the offshore side of the domain (Figure 10f) can be explained by the fact that potential vorticity is mostly conserved in this region, except near the Tasman Front. Since $\partial\rho/\partial z$ does not show any significant changes in this region, poleward movement requires an increase in relative vorticity and equatorward movement a decrease in relative vorticity to conserve PV (see equation (1)). This is in agreement with the meandering behavior of the Tasman Front [*Tilburg et al*., 2001] and the changes in relative vorticity seen in Figure 10f.

South of 32°S the pattern of the Lagrangian changes in potential vorticity is reversed, with increasing values of potential vorticity along the coastline and decreasing values offshore (Figure 10a). This pattern can be explained

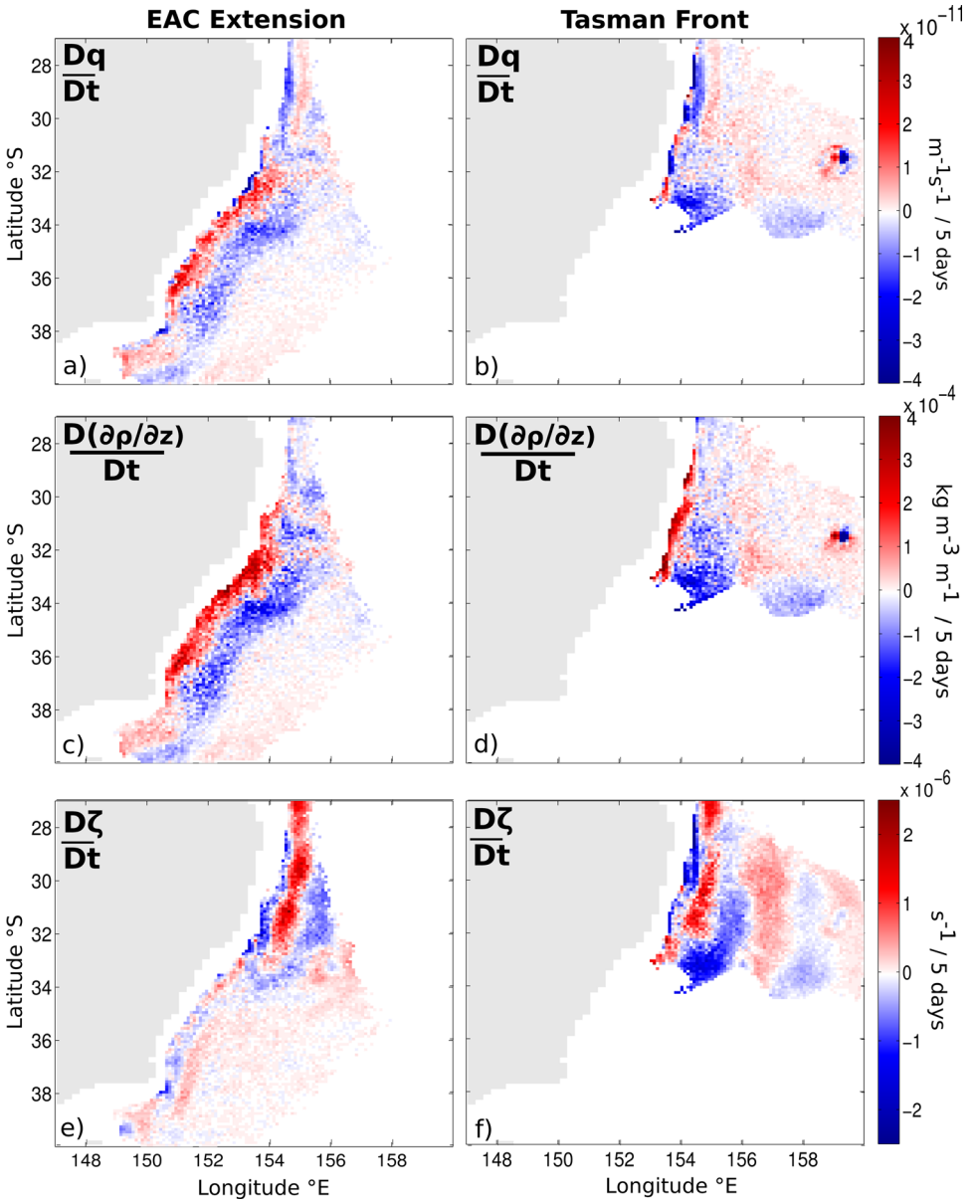

Figure 10. The material derivative of potential vorticity (q), the stratification ($\partial\rho/\partial z$), and relative vorticity (ζ) per 5 days, for particles following the extension of the EAC (left column) and particles following the Tasman Front (right column). The material derivative is calculated by using first-order differencing over a 5 day time window and is averaged over a random sample of 100 particles per grid box located between 350 and 450 m depth. Note that all terms have different units.

by the changes seen in the $\partial\rho/\partial z$ term (Figure 10c). Particles feel a stretching of isopycnals when they travel close to the coast along their trajectory and a squeezing offshore. The signal follows the coastline closely and the width of the region where the changes take place is about 200 km. Since southward traveling eddies take exactly this route they might induce the pattern seen here. Anticyclonic eddy motion is southward near the coast and northward offshore. The cross-shore component cancels out in the mean as an eddy moves south. However, the alongshore component can cause an increase (decrease) in potential vorticity at the onshore (offshore) side of the eddy, due to a decrease (increase) in the stratification magnitude seen in Figure 10c.

5. Discussion

In this paper we have used Lagrangian particles advected in the Modular Ocean Model to investigate where and how the fate of the particles following the EAC extension and the Tasman Front is controlled. We have

seen that the pathway of the particles downstream of the separation is to some extent already determined by the particles' distribution within the EAC current upstream of the separation latitude, where the surface waters follow the Tasman Front and the deeper waters follow the extension of the EAC. In the region where the two water masses overlap, at 400 m depth, the fate of the water seems to depend on the presence of anticyclonic eddies that push the isopycnals down enabling particles to travel further south.

The fact that the Tasman Front pathway is fed by water from the top 600 m of the EAC agrees well with the observations by *Sutton and Bowen* [2014]. Furthermore, this study shows that the water located deeper in the EAC is indeed traveling southward as hypothesized by *Sutton and Bowen* [2014]. We have seen that the particles traveling southward below 600 m depth do not significantlyt change their depth in the water column, whereas particles traveling in the upper 600 m are slightly advected upward. This might have implications for the nutrient variability south of the separation point. Studying the change in density of the particles between 27°S and 40°S shows that the vertical displacement is due to the adiabatic behavior of the particles. Particles following the Tasman Front keep their density constant by veering eastward instead of displacing vertically.

The results of this study show that the structure of the isopycnals is dominant in splitting the two pathways. Particles traveling below 600 m do not experience a strong vertical change in the isopycnal which they are following and are therefore able to continue their journey southward along the eastern boundary of Australia. Particles in the upper 600 m however experience a strong horizontal gradient in the density field around the separation latitude, due to the outcropping of isopycnals, and most of the particles are forced to continue their journey eastward.

Vertical and horizontal shifts in the pycnocline could explain the anomalies seen in the stratification and potential vorticity. From the results, it is also clear that layer thickness variations are dominating the structure of potential vorticity in this region. The vertical downward shift of the pycnocline is explained by the increased anticyclonic behavior around the separation latitude in Figure 9h. This could mean that anticyclonic eddies are essential for transporting water across the horizontal gradient in density in the top layer. The negative anomaly in the stratification for particles following the Tasman Front could be explained by the southward movement of the slope of the pycnocline. The movement of the front is related to the separation latitude of the EAC and since time series of the separation latitude show a clear seasonal cycle, one would expect a seasonal signal in the number of particles moving eastward as well. However, there is no clear seasonal signal seen in the number of particles following the Tasman Front (Figure 8a) and further investigation is necessary to see what is causing the anomaly in stratification.

The fact that anticyclonic eddies play a crucial role in the transport southward in the upper layer connects well with the results seen in the seasonal dependence of the transport southward (Figure 8a) in relation to the seasonal pattern seen in the eddy activity (Figure 3c). Furthermore, the way the EAC separation takes place is favorable for generating anticyclonic eddies. *Cetina-Heredia et al*. [2014] have looked at the amount of southward transport that takes place inside eddies and estimate that only 15.8 $\pm$ 18.3% of the transport takes place within eddies. However, this is calculated with respect to the total transport southward, and not with respect to the transport taking place in the upper 600 m. The transport southward originating from the upper layer of the EAC might show a larger percentage of water being transported inside eddies as the eddies are surface-intensified.

This paper is one of the first attempts to investigate the conservation of potential vorticity from a Lagrangian perspective in a general circulation ocean model. North of the separation latitude, an increase in cyclonic and anticyclonic behavior is observed downstream. As a result, the potential vorticity is decreasing at the cyclonic (onshore) side and increasing at the anticyclonic (offshore) side of the flow. This in good agreement with the results found by *Kiss* [2010] that changes downstream in PV are due to changes in relative vorticity rather than changes in stratification. The loss of cyclonic relative vorticity, appearing as a region of positive $D\zeta/Dt$, just prior to separation at 153.5°E and 33°S in Figure 10f is also characteristic of the mechanisms of *Kiss* [2002, 2010], but further investigation is beyond the scope of this paper.

In this study, only the vertical component of the Ertel potential vorticity equation is considered. However, since we have seen that a steep slope in the pycnocline is observed at the separation latitude, the horizontal component (the baroclinic term) of the Ertel potential vorticity equation (given by $\boldsymbol{\omega}_h \cdot \nabla_h(-\rho/\rho_0)$, where $\boldsymbol{\omega}_h$ is the horizontal component of the absolute vorticity $\boldsymbol{\omega}=f\hat{\boldsymbol{k}}+\nabla\times\boldsymbol{u}$) might not be negligible in

this region [*Holmes et al.*, 2014]. Indeed, *Godfrey et al.* [1980b] find low Richardson numbers at the separation latitude indicating that horizontal density gradients and shear might be of importance. Consequently, the regions where we see nonconservation of PV in Figure 10 could still be conserving the full potential vorticity when including the baroclinic term.

To assess whether friction, diabatic processes or the horizontal component of the Ertel PV are causing the potential vorticity to change along a particles' trajectory, the vorticity balance has to be investigated. For this, an online assessment of the different potential vorticity terms is necessary to ensure a closing balance and the results would benefit from a higher temporal and horizontal resolution of the ocean model. A higher horizontal resolution would also result in a more realistic representation of the eddy field and a higher temporal and horizontal resolution would decrease the errors made when interpolating the potential vorticity fields to the particle location and moment in time. Nevertheless, our eddy-permitting results are useful for understanding ocean dynamics in the latest generation (CMIP6) of the climate models.

Acknowledgments
This project was supported by the Australian Research Council via grant DE130101336 and, in part, via grant CE110001028. Sea surface height from the Archiving Validation and Interpretation of Satellite Oceanographic (AVISO) data were obtained from http://www.aviso.oceanobs.com/duacs. P. Spence was supported by the Australian Research Council via grant DE150100223. We thank both reviewers for helpful comments which improved this paper.

References

Bostock, H. C., B. N. Opdyke, M. K. Gagan, A. E. Kiss, and L. K. Fifield (2006), Glacial/interglacial changes in the East Australian current, *Clim. Dyn.*, *26*, 645–659.
Bowen, M., J. L. Wilkin, and W. J. Emery (2005), Variability and forcing of the East Australian Current, *J. Geophys. Res.*, *110*, C03019, doi:10.1029/2004JC002533.
Cetina-Heredia, P., E. van Sebille, and M. A. Coleman (2014), Long-term trends in the East Australian Current separation latitude and eddy driven transport, *J. Geophys. Res. Oceans*, *119*, 4351–4366, doi:10.1002/2014JC010071.
Chassignet, E. P., and D. P. Marshall (2008), Gulf stream separation in numerical ocean models, in *Ocean Modeling in an Eddying Regime*, edited by M. W. Hecht and H. Hasumi, pp. 39–61, AGU, Washington, D. C.
Condie, S. A., and J. R. Dunn (2006), Seasonal characteristics of the surface mixed layer in the Australasian region: Implications for primary production regimes and biogeography, *Mar. Freshwater Res.*, *57*(6), 569–590.
Cushman-Roisin, B., and J. Beckers (2011), *Introduction to Geophysical Fluid Dynamics: Physical and Numerical Aspects*, vol. 101, Academic Press, Amsterdam, Netherlands.
Delworth, T., et al. (2012), Simulated climate and climate change in the GFDL CM2.5 high-resolution coupled climate model, *J. Clim.*, *25*, 2755–2781.
Dijkstra, H. A. (2008), *Dynamical Oceanography*, Springer, Berlin.
Dunn, J. R., and K. R. Ridgway (2002), Mapping ocean properties in regions of complex topography, *Deep Sea Res., Part I*, *49*(3), 591–604.
Everett, J. D., M. E. Baird, P. R. Oke, and I. M. Suthers (2012), An avenue of eddies: Quantifying the biophysical properties of mesoscale eddies in the Tasman Sea, *Geophys. Res. Lett.*, *39*, L16608, doi:10.1029/2012GL053091.
Farneti, R., T. Delworth, A. Rosati, S. Griffies, and F. Zeng (2010), The role of mesoscale eddies in the rectification of the Southern Ocean response to climate change, *J. Phys. Oceanogr.*, *40*, 1539–1557.
Godfrey, J. S., G. R. Cresswell, T. J. Golding, and A. F. Pearce (1980a), The separation of the East Australian Current, *J. Phys. Oceanogr.*, *10*, 430–439.
Godfrey, J. S., G. R. Cresswell, and F. M. Boland (1980b), Observations of low Richardson numbers and undercurrents near a front in the East Australian Current, *J. Phys. Oceanogr.*, *10*, 301–307.
Griffies, S., et al. (2009), Coordinated ocean-ice reference experiments (COREs), *Ocean Modell.*, *26*, 1–46.
Hill, K. L., S. R. Rintoul, K. R. Ridgway, and P. R. Oke (2011), Decadal changes in the South Pacific western boundary current system revealed in observations and ocean state estimates, *J. Geophys. Res.*, *116*, C01009, doi:10.1029/2009/JC005926.
Hobday, A. J., and K. Hartmann (2006), Near real-time spatial management based on habitat predictions for a longline bycatch species, *Fish. Manage. Ecol.*, *13*, 365–380.
Holmes, R. M., L. N. Thomas, L. Thompson, and D. Darr (2014), Potential vorticity dynamics of tropical instability vortices, *J. Phys. Oceanogr.*, *44*(3), 995–1011.
Kiss, A. E. (2002), Potential vorticity "crises," adverse pressure gradients, and western boundary current separation, *J. Mar. Res.*, *60*, 779–803.
Kiss, A. E. (2010), Dynamics of separating western boundary currents in ocean models, in *IOP Conference Series: Earth and Environmental Science*, IOP Publishing, *11*(1), 012034 pp., doi:10.1088/1755-1315/11/1/012034.
Large, W., and S. Yeager (2009), The global climatology of an interannually varying air–sea flux data set, *Clim. Dyn.*, *33*, 341–364.
Marchesiello, P., and J. H. Middleton (2000), Modeling the East Australian Current in the Western Tasman Sea, *J. Phys. Oceanogr.*, *30*, 2956–2971.
Mata, M. M., S. E. Wijffels, J. A. Church, and M. Tomczak (2006), Eddy shedding and energy conversions in the East Australian Current, *J. Geophys. Res.*, *111*, C09034, doi:10.1029/2006JC003592.
Nakano, H., H. Tsujino, and R. Furue (2008), The Kuroshio Current System as a jet and twin "relative" recirculation gyres embedded in the Sverdrup circulation, *Dyn. Atmos. Oceans*, *45*(3–4), 135–164.
Oliver, E. C. J., and N. J. Holbrook (2014), Extending our understanding of South Pacific gyre "spin up": Modeling the East Australian Current in a future climate, *J. Geophys. Res. Oceans*, *119*, 2788–2805, doi:10.1002/2013JC009591.
Paris, C. B., J. Helgers, E. van Sebille, and A. Srinivasan (2013), The connectivity modelling system: A probabilistic tool for the multi-scale tracking of biotic and abiotic variability in the ocean, *Environ. Modell. Software*, *42*, 47–54.
Qin, X., E. van Sebille, and A. S. Gupta (2014), Quantification of errors induced by temporal resolution on Lagrangian particles in an eddy-resolving model, *Ocean Modell.*, *76*, 20–30.
Qiu, B., and S. Chen (2004), Seasonal modulations in the eddy field of the South Pacific Ocean, *J. Phys. Oceanogr.*, *34*(7), 1515–1527.
Ridgway, K. R., and J. R. Dunn (2003), Mesoscale structure of the East Australian Current System and its relationship with topography, *Prog. Oceanogr.*, *56*, 189–122.
Ridgway, K. R., and J. S. Godfrey (1994), Mass and heat budgets in the East Australian Current System: A direct approach, *J. Geophys. Res.*, *99*(C2), 3231–3248.

Ridgway, K. R., and J. S. Godfrey (1997), Seasonal cycle of the East Australian Current, *J. Geophys. Res.*, *102*(C10), 22,921–22,936.
Ridgway, K. R., J. R. Dunn, and J. Wilkin (2002), Ocean interpolation by four-dimensional weighted least squares-application to the waters around Australasia, *J. Atmos. Oceanic Technol.*, *19*(9), 1357–1375.
Roughan, M., P. R. Oke, and J. H. Middleton (2003), A modeling study of the climatological current field and the trajectories of upwelled particles in the East Australian Current, *J. Phys. Oceanogr.*, *33*(12), 2551–2564.
Schaeffer, A., M. Roughan, and B. D. Morris (2013), Cross-shelf dynamics in a western boundary current regime: Implications for upwelling, *J. Phys. Oceanogr.*, *43*(5), 1042–1059.
Scharffenberg, M. G., and D. Stammer (2010), Seasonal variations of the large-scale geostrophic flow field and eddy kinetic energy inferred from the TOPEX/poseidon and Jason-1 tandem mission data, *J. Geophys. Res.*, *115*, C02008, doi:10.1029/2008JC005242.
Sloyan, B. M., and T. J. O'Kane (2015), Drivers of decadal variability in the Tasman Sea, *J. Geophys. Res. Oceans*, *120*, 3193–3210, doi:10.1002/2014JC010550.
Sutton, P. J. H., and M. Bowen (2014), Flows in the Tasman Front south of Norfolk Island, *J. Geophys. Res. Oceans*, *119*, 3041–3053, doi:10.1002/2013JC009543.
Thompson, K. R., and E. Demirov (2006), Skewness of sea level variability of the world's oceans, *J. Geophys. Res.*, *111*, C05005, doi:10.1029/2004JC002839.
Tilburg, C. E., H. E. Hulburt, J. J. O'Brien, and J. F. Shriver (2001), The dynamics of the East Australian Current System: The Tasman Front, the East Auckland Current, and the East Cape Current, *J. Phys. Oceanogr.*, *31*(10), 2917–2943.
Van Sebille, E., M. H. England, J. D. Zika, and B. M. Sloyan (2012), Tasman leakage in a fine-resolution ocean model, *Geophys. Res. Lett.*, *39*, L06601, doi:10.1029/2012GL051004.
Zlotnicki, V., L. L. Fu, and W. Pratzert (1989), Seasonal variability in global sea level observed with Geosat altimetry, *J. Geophys. Res.*, *94*(C12), 17,959–17,969.